Original Article

JCBFM

Journal of Cerebral Blood Flow & Metabolism
2017, Vol. 37(6) 1944–1958

DOI: 10.1177/0271678X16657573
journals.sagepub.com/home/jcbfm
SAGE

Planning-free cerebral blood flow territory mapping in patients with intracranial arterial stenosis

Daniel F Arteaga[1], Megan K Strother[1], L Taylor Davis[1], Matthew R Fusco[2], Carlos C Faraco[1], Brent A Roach[1], Allison O Scott[1] and Manus J Donahue[1,3,4,5]

Abstract

A noninvasive method for quantifying cerebral blood flow and simultaneously visualizing cerebral blood flow territories is vessel-encoded pseudocontinuous arterial spin labeling MRI. However, obstacles to acquiring such information include limited access to the methodology in clinical centers and limited work on how clinically acquired vessel-encoded pseudocontinuous arterial spin labeling data correlate with gold-standard methods. The purpose of this work is to develop and validate a semiautomated pipeline for the online quantification of cerebral blood flow maps and cerebral blood flow territories from planning-free vessel-encoded pseudocontinuous arterial spin labeling MRI with gold-standard digital subtraction angiography. Healthy controls (n = 10) and intracranial atherosclerotic disease patients (n = 34) underwent 3.0 T MRI imaging including vascular (MR angiography) and hemodynamic (cerebral blood flow-weighted arterial spin labeling) MRI. Patients additionally underwent catheter and/or CT angiography. Variations in cross-territorial filling were grouped according to diameters of circle of Willis vessels in controls. In patients, Cohen's *k*-statistics were computed to quantify agreement in perfusion patterns between vessel-encoded pseudocontinuous arterial spin labeling and angiography. Cross-territorial filling patterns were consistent with circle of Willis anatomy. The intraobserver Cohen's *k*-statistics for cerebral blood flow territory and digital subtraction angiography perfusion agreement were 0.730 (95% CI = 0.593–0.867; reader one) and 0.708 (95% CI = 0.561–0.855; reader two). These results support the feasibility of a semiautomated pipeline for evaluating major neurovascular cerebral blood flow territories in patients with intracranial atherosclerotic disease.

Keywords

Angiography, cerebral blood flow territory, circle of Willis, collaterals, MRI, vessel-encoded arterial spin labeling, arterial spin labeling, atherosclerosis, cerebrovascular disease, imaging, MR angiography, neuroradiology

Received 16 October 2015; Revised 29 April 2016; Accepted 23 May 2016

Introduction

Intracranial atherosclerotic disease (ICAD) is a well-known risk factor for stroke.[1] In contrast to acute arterial occlusions caused by abrupt plaque rupture, occlusions caused by progressive narrowing of intracranial arterial vessels may be associated with preserved downstream perfusion due to the gradual formation of collateral pathways.[2] Thus, the extent of collateralization in ICAD patients may serve as an important biomarker of stroke risk and may have prognostic potential for titrating aggressive preventative therapies to the most high-risk patients.[3]

Digital subtraction angiography (DSA) is currently the gold standard for examining cerebral vasculature,

[1]Radiology, Vanderbilt University Medical Center, Nashville, USA
[2]Neurosurgery, Vanderbilt University Medical Center, Nashville, USA
[3]Psychiatry, Vanderbilt University Medical Center, Nashville, USA
[4]Physics and Astronomy, Vanderbilt University, Nashville, USA
[5]Neurology, Vanderbilt University Medical Center, Nashville, USA

Corresponding author:
Manus J Donahue, Vanderbilt University Institute of Imaging Science, 1161 21st Ave S, MCN, AAA-3115 Nashville, TN 37232–2310, USA.
Email: mj.donahue@vanderbilt.edu

including the evaluation of collateral flow through the circle of Willis and leptomeningeal vessels. However, DSA is invasive, limiting its availability for routine long-term monitoring or surveillance. A noninvasive method for evaluating collateralization at the tissue level is vessel-encoded pseudocontinuous arterial spin labeling (VE-pCASL).[4] Here, blood water in the internal carotid arteries (ICAs) and vertebrobasilar artery (VBA) is magnetically labeled and individual CBF territories are subsequently calculated from the relative attenuation in the tissue water signal following the different tagging conditions. Limitations of VE-pCASL protocols include expertise required in planning and analysis, as well as limited information on consistency between gold-standard DSA and VE-pCASL in intracranial stenosis patients. Several VE-pCASL protocols have recently been evaluated which do not require planning,[5,6] including in patients with cerebrovascular disease[7]; however, these planning-free sequences have not yet been directly compared with DSA. While two studies have found good correspondence between VE-ASL data and DSA,[8,9] they require user planning that may not be reasonable within the time constraints of clinical brain MR protocols or without more advanced training in these procedures for hospital technologists. Therefore, efforts are needed to extend this work to generate a clinically feasible protocol from which collateralization can be visualized in a short time frame and in the same session as standard clinical imaging.

Here, we build upon this work by presenting a semi-automated pipeline for quantifying CBF territory maps from a planning-free VE-pCASL MRI sequence implemented on clinical scanners in a short time frame of less than 5 min. Specifically, we aimed to develop an optimized analysis routine and understand whether this planning-free approach: (i) correctly identified asymmetric flow territories secondary to normal circle of Willis variants in healthy volunteers, (ii) correctly identified collateralization from DSA in subjects with severe ICAD, and (iii) provided asymmetric flow territory patterns consistent with vasculopathy extent in subjects with symptomatic moderate and severe ICAD. The results of this study are intended to better inform best practices for planning-free VE-pCASL acquisition and analysis in the clinical setting, as well as to outline the current strengths and remaining limitations of this method for routine use.

Materials and methods

Patient anonymity, informed consent, and ethics

All study components were reviewed and approved by the Vanderbilt University Institutional Review Board. Procedures were followed in accordance with the ethical standards of the Vanderbilt University Human Research Protection Program and the Helsinki Declaration of 1975 (and as revised in 1983). All components of this study were in compliance with the Health Insurance Portability and Accountability Act.

Participant demographics and stenosis measurements

Healthy volunteers ($n = 10$; age $= 33.2 \pm 8.0$ yrs; 5 M/5F) without known cerebrovascular disease and subjects presenting with angiographically confirmed atherosclerotic stenosis of intracranial vessels or intracranial segments of the ICAs and VBA ($n = 34$; age $= 60.7 \pm 12.4$ yrs; 16 M/18F) were enrolled between 1 August 2013 and 1 June 2015 and provided informed, written consent. Healthy volunteers were not age matched to ICAD subjects as the purpose of their inclusion was only to measure the sensitivity of the VE-pCASL approach to circle of Willis variations in the absence of ICAD, and there was concern that an older, age-matched cohort would have varying degrees of vasculopathy that could confound the analysis. Twenty-nine of 34 patients had prior infarcts; the remaining five experienced TIA prior to study enrollment (see Table 1).

Experimental imaging

All participants were scanned at 3.0T (Philips Medical Systems; Best, The Netherlands). All ICAD subjects additionally underwent clinically acquired CT angiography (CTA). Ten of these ICAD subjects also underwent DSA within 40 days of the VE-pCASL MRI. Standard T_1-weighted (3D turbo-gradient echo; TR/TE = 8.9/4.6 ms; spatial resolution = 1 mm × 1 mm × 1 mm), T_2-weighted fluid attenuated inversion recovery, FLAIR (turbo spin echo; TR/TE = 11,000/120 ms; spatial resolution = 1.9 mm × 1.9 mm × 5 mm) imaging, and 3D time-of-flight magnetic resonance angiography (MRA; 3D gradient echo; TR/TE = 13.8/1.8 ms; spatial resolution = 1.3 mm × 1.3 mm × 1 mm) sequences were performed in addition to VE-pCASL acquisitions (single-shot gradient echo EPI; TR/TE/PLD = 3900/13/1650 ms; spatial resolution = 3 mm × 3 mm × 7 mm, labeling offset from AC/PC line = −90 mm, SENSE factor = 2.5). The VE-pCASL sequence employed a 1650 ms labeling pulse train consisting of 0.7 ms Hanning-windowed pulses with an interpulse gap of 0.7 ms (Figure S1A). The only user input required to run the VE-pCASL MRI protocol was positioning of the imaging volume. Separate labeling of the left ICA (LICA), right ICA (RICA), and vertebral arteries was performed for each participant, yielding three CBF territories except in the case of occlusions proximal to the tagging plane that

Table 1. Characteristics of patients with intracranial stenosis.

Age (yrs)	Sex	DSA	Asym. Ind.	Circle of Willis	Stenosis	Prior infarcts
Moderate Stenosis (50–69%)/Complete circle of Willis (excluding PCOM)						
49	M	N	3.3	Complete COW	63% R M1	R basal ganglia, R posterior fossa
71	F	N	3.5	Absent R/L PCOM	55% R M1	R MCA cortical
38[a]	F	Y	2.8	Complete COW	67% L M1	L MCA cortical
71	F	N	4.0	Complete COW	55% basilar, 50% LICA	R PCA
61	M	N	5.8	Complete COW	60% LICA	R basal ganglia, L thalamus
73	M	N	5.8	Complete COW	50% R M2	R subinsular
38	F	N	4.9	Complete COW	67% R M1	R MCA cortical, R basal ganglia
66	M	N	1.6	Complete COW	60% L P1	
66	F	N	4.2	Complete COW	61% R vert	
66	M	N	4.7	Complete COW	59% L M1, 57% R vert	L anterior/posterior watershed
72	F	N	0.8	Complete COW	67% RICA	R PCA
73[a]	M	Y	3.8	Complete COW	63% R vert, 50% R M1	R/L basal ganglia, R/L posterior fossa, R/L corona radiata
Mean ± SE			**Mean ± SE**		**Mean ± SE**	
59.1 ± 6.0			3.8 ± 0.4		60.6 ± 1.5	
Severe Stenosis (70–100%)/Incomplete circle of Willis (excluding PCOM)						
51[a]	M	Y	5.6	Complete COW	79% L M2	R/L corona radiata
34[a]	M	Y	5.6	Absent R/L PCOM	72% LICA, 61% RICA	
73	F	N	4.4	Absent R PCOM	73% R M1	R/L basal ganglia, R deep watershed
51[a]	M	Y	2.6	Complete COW	79% R M1	R posterior watershed, R basal ganglia, R PCA
72	M	N	10.6	Left fetal PCOM	100% L P1, 67% R vert, 53% RICA	L posterior fossa
69	M	N	2.1	Complete COW	99% R M1	R MCA cortical, L subinsular
52	F	N	17.9	Complete COW	99% L M2, 57% LICA, 50% RICA	R basal ganglia
57	M	N	20.8	Absent R A1	100% R A1, 80% basilar	R anterior watershed, L deep watershed
53[a]	M	Y	10.9	Complete COW	81% LICA	L anterior watershed, L MCA cortical
82	F	N	4.6	Absent R A1	100% R A1, 65% R M2	R posterior watershed, R MCA cortical
75	F	N	13.2	Complete COW	100% R P2	R PCA
73	F	N	4.5	Complete COW	72% basilar	R posterior fossa, L basal ganglia
68	F	Y	1.6	Complete COW	99% L M1	L basal ganglia
49	F	N	2.1	Fetal R/L PCOM	100% R/L P1, 81% RICA	R anterior/posterior watershed, R PCA, R posterior fossa

(continued)

Table 1. Continued

Age (yrs)	Sex	DSA	Asym. Ind.	Circle of Willis	Stenosis	Prior infarcts
51[a]	M	N	19.0	Absent L A1	100% L A1, 68% basilar	L thalamus
53	F	N	8.8	Absent L PCOM	100% R P1	L thalamus
64[a]	F	Y	12.7	Absent L PCOM	62% RICA, 53% LICA	R MCA cortical, R basal ganglia
64	F	N	4.1	Complete COW	82% basilar	
68[a]	M	Y	N/A	Absent R PCOM	100% R supraclinoid ICA	
62	M	N	N/A	Absent ACOM	100% L paraclinoid ICA	L anterior/posterior watershed
62[a]	F	Y	N/A	Complete COW	100% L paraclinoid ICA	R anterior watershed, L MCA cortical
Mean ± SE			**Mean ± SE**		**Mean ± SE**	
61.1 ± 2.5			8.4 ± 1.5		90.3 ± 2.8	
Failed analysis due to motion						
38	F	N	N/A	Complete COW	68% L M1	L MCA cortical

[a]Denotes that patient also underwent DSA

A1: first segment of anterior cerebral artery; Asym. Ind.: asymmetry index: measure of CBF territory asymmetry relative to complete circle of Willis; COW: circle of Willis; DA: digital subtraction angiography; ICA: internal carotid artery; M1: first segment of middle cerebral artery; M2: second segment of middle cerebral artery; MCA: middle cerebral artery; P1: first segment of posterior cerebral artery; P2: second segment of posterior cerebral artery; PCA: posterior cerebral artery; PCOM: posterior communicating artery; L: left; R: right; SE: standard error; Vert: vertebral artery.

were detected previously with angiography data, in which case two CBF territories were used. The following five labeling scenarios were employed in an automated fashion: (i) no label (control), (ii) nonselective label, (iii) labeling with 25 mm between full label and control in the R/L direction, (iv) labeling with 9 mm between full label and control in the A/P direction, and (v) labeling with 9 mm between full label and control in the A/P direction shifted by 4.5 mm anteriorly (Figure S1B). Of note, the purpose of labeling scenarios (iv) and (v) was to separate the anterior circulation from the posterior circulation, rather than to separate the vertebral arteries. In patients, a separate equilibrium magnetization (M_0) image was acquired with an identical spatial resolution and readout as the VE-pCASL scan but with TR = 20 s and all spin labeling pulses removed. Total protocol duration, including M_0 image acquisition, was approximately 4 min 50 s.

Angiographic evaluation of healthy control and patient data

All MRA, CTA, and DSA data were evaluated by a board-certified neuroradiologist (MKS; experience = 12 yrs) blinded to clinical history. In healthy controls, the maximum diameters of bilateral A1, P1, and PCOM vessels were measured from MRA source sequences using OsiriX Imaging Software (Pixmeo, Geneva, Switzerland).[10] Stenosis degree in ICAD subjects was obtained using previously published guidelines[11] and determined from vascular imaging acquired within 30 days of hemodynamic MRI in the following order: (i) from clinical DSA if available; (ii) if no DSA, from clinical CTA; (iii) if no CTA, from MRA. Only stenoses with luminal diameter narrowing $\geq 50\%$ were considered potentially flow limiting. ICAD subjects were grouped according to whether they had moderate stenosis (50–69%) or severe steno-occlusion (70–100%) of at least one of the above intracranial vessels.

Processing and analysis of VE-pCASL data

VE-pCASL analysis was performed in Python using the Vanderbilt ASL Toolkit (Nashville, TN, USA; available for download at http://www.nitrc.org/projects/vandpire). VE-pCASL data from all subjects were corrected for motion and spatially smoothed (full-width-half-maximum = 0.93 mm). Data were then pair-wise subtracted and normalized by the M_0 value to generate CBF-weighted maps. As healthy controls did not have M_0 images, the control image was used for normalization, which was scaled by $1\text{-}e^{(-TR/T1t)}$ to account for the steady-state effects of the excitation pulse, where $T1_t = 1200$ ms is the T1 of tissue at 3 T. Note that as the topic of the study was flow territory quantification, rather than absolute CBF, this discrepancy is not

intended to bias the results presented (see "Discussion" section). CBF was quantified assuming a blood water $T_1 = 1.65$ s and in accord with the recent guidelines of the ISMRM perfusion study group.[4] CBF territory maps were calculated using (i) an unsupervised *k*-means algorithm[12] and separately using (ii) a fuzzy *c*-means clustering algorithm.[13] Unlike the *k*-means algorithm which can only assign a voxel to a single vascular territory, the fuzzy *c*-means algorithm assigns voxels three values from 0 to 1 based upon the relative perfusion contributed by each of the three major vascular territories and thus has the added capability of detecting mixing between CBF territories. For both algorithms, the number of clusters (i.e. vascular territories) was set to three (left ICA, right ICA, and VBA territories) except when there was a known occlusion based upon angiography data, in which the number of clusters was set to two. Input data were normalized by dividing the selectively labeled images by the CBF-weighted image (resulting from the subtraction of the global label condition from the control condition), yielding three relative labeling efficiency maps. These maps were then thresholded to exclude voxels with quantified cortical CBF values at the noise level of 25 ml/100 g/min, which was based on known thresholds of viable tissue. The *k*-means++ algorithm[14] was used for initial seeding for the *k*-means algorithm. To guide both the *k*-means algorithm and the fuzzy *c*-means clustering algorithm, a CBF territory probability map derived from 50 healthy subjects in 2 mm MNI space was back-registered to native space for every participant and supplied as a template for spatial weighting. For every voxel in this CBF territory probability map, three values were assigned between 0 and 1 corresponding to the mean likelihood that the voxel belonged to each of the three major flow territories. An additional spatial weighting factor was multiplied by these probability values to increase the influence that they had in determining the final CBF territories. Thus, six features were provided for each voxel: three labeling efficiency values corresponding to the labeling data acquired in the R/L and two A/P directions, and three probability values multiplied by a spatial weighting factor corresponding to the prior likelihood that a voxel belonged to a particular CBF territory. Optimal spatial weighting factors were investigated in this study.

Two postprocessing steps were additionally applied to the mixing CBF territory maps derived from the fuzzy *c*-means algorithm. First, mixing voxels were assigned only when the highest relative CBF value for a given territory was no more than twice the second highest value. For example, CBF values of 0.3 for RICA and 0.6 for LICA would meet the minimum criteria for RICA–LICA mixing. Next, to separate informative data from noise, mixing voxel cluster sizes were thresholded to a minimum of eight contiguous voxels. Voxels that did not meet both of these criteria were designated to a single vascular territory according to the highest relative perfusion contribution. These mixing criteria were determined empirically after comparing mixing CBF territory maps with mixing patterns observed on DSA.

Optimization of spatial weighting

To optimize the CBF territory results, multiple spatial weighting factors were evaluated in both healthy controls and ICAD subjects. The goal of this analysis was to determine the highest spatial weighting factor that accurately reflected circle of Willis anatomy on an individual basis. While low spatial weighting factors may be less robust in characterizing regions with poor data quality or hypoperfusion, high values may over-weight the spatial prior information relative to the actual data. Notably, only nonmixing CBF territory maps were used for this analysis, as their patterns are ideal for validation.

First, in a single healthy control with known aplastic right A1 and P1 segments, CBF territory maps were evaluated for a range of spatial weighting factors. The extent of collateralization was quantitatively determined in the following manner. A standard CBF territory map was calculated (Figure S2) by inputting the prior spatial CBF territory probability map without VE-pCASL data into the clustering algorithm. Next, the extent of cross-territorial filling was determined by calculating the number of voxels overlapping with a different territory on the standard CBF territory map. Specifically, the number of LICA voxels overlapping with the VBA and RICA territories on the standard map was divided by the total number of voxels in the VBA and RICA standard territories, respectively, and multiplied by 100 to obtain an overlap percentage. This procedure was also performed for RICA voxels, yielding four measures per subject, and is referred to as the *cross-territorial index* (see Figure 1(a)). This process yielded four overlap combinations to account for all major circle of Willis collateralization patterns. Notably, two additional *cross-territorial indices,* corresponding to the number of VBA voxels overlapping with the LICA and RICA territories separately, were only calculated for participants with DSA as it is difficult to infer posterior perfusion patterns for subjects with large P1 segments of the posterior cerebral artery (PCA) based upon CTA or MRA data alone. For this healthy control, *cross-territorial indices* were calculated for five different spatial weighting factors, as shown in Figure 1(b). Figure 1(c) visually demonstrates the extent of cross-territorial filling for these five spatial weighting factors in the same subject. A conservative spatial weighting factor ≤ 1.3 was used for subsequent analysis.

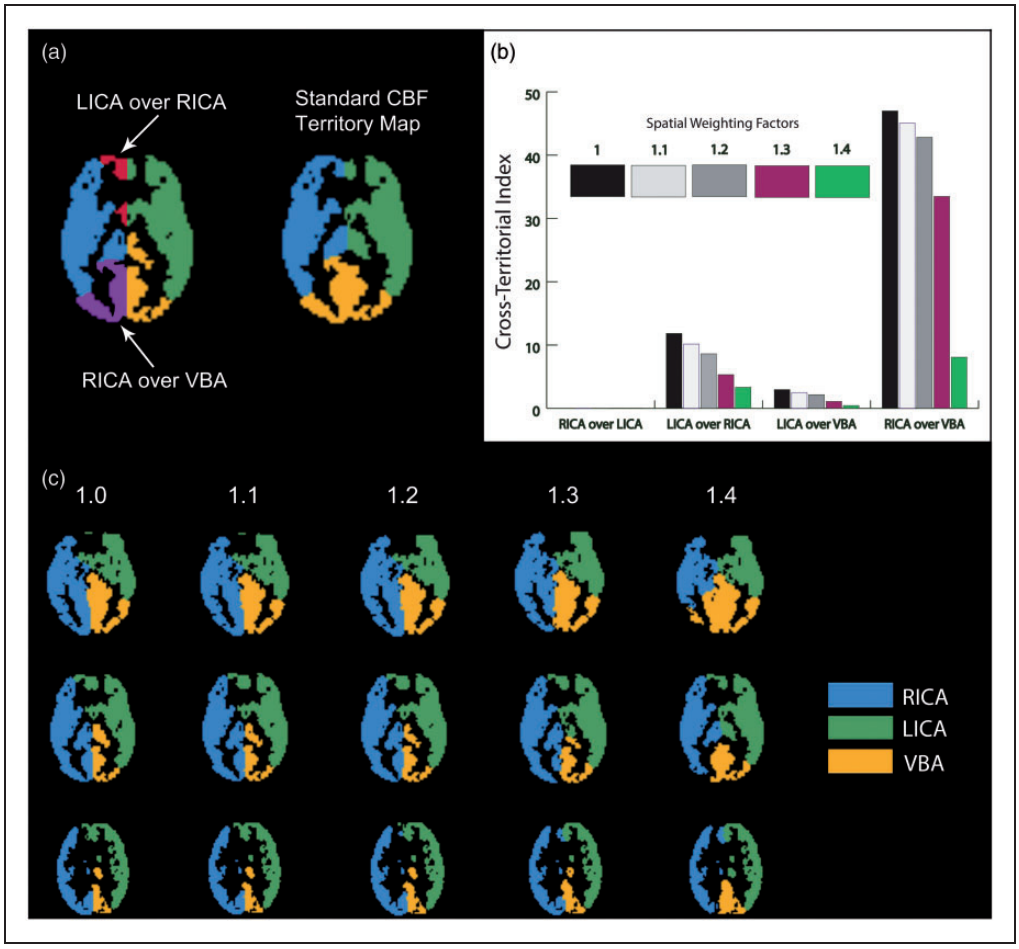

Figure 1. Example of how the *cross-territorial index* is calculated in a healthy control with aplastic right A1 and aplastic right P1 vessels. (a) Left: When considering the right hemisphere, LICA voxels overlapping with RICA voxels in the standard CBF territory map are shown in red, and RICA voxels overlapping with VBA voxels are shown in purple. Right: The standard CBF territory map in this subject's native space. As a result of the coregistration process, small differences exist between the two maps with regards to the total number of voxels shown. (b) To optimize the k-means analysis, spatial weighting parameters were evaluated in the same control by quantifying the extent of cross-territorial filling. The goal of this analysis was to identify the highest possible spatial weighting factor that also accurately reflected the anatomy, in order to produce robust results in patients. (c) Qualitative cross-territorial filling analysis, which corresponds with the quantitative analysis above, shown across three slices in the brain for multiple spatial weighting factors.

While these results may have been extrapolated across healthy subjects that are expected to have CBF territory maps with relatively high signal-to-noise ratios (SNR), extrapolation across ICAD patients was more uncertain. Specifically, we hypothesized a need to increase spatial weighting in ICAD CBF territory maps that may have larger regions of hypoperfusion and lower SNR. Thus, the relationship between SNR and the maximum spatial weighting factor values producing accurate CBF territory maps was calculated. For all subjects, 27 contiguous voxels (equivalent to a 3D cube) that exceeded the 25 ml/100 g/min noise level threshold in the CBF map were used to calculate SNR. A single signal value was first obtained by averaging voxel-wise signal values across all 27 contiguous voxels and dynamics. Noise was determined by obtaining the absolute difference in signal values between adjacent dynamics for each voxel and then calculating the mean of these values across all 27 contiguous voxels and dynamics. The final SNR for each subject was estimated as follows: (signal $\times \sqrt{}$(number of dynamics))/noise. CBF territory maps for a range of spatial weighting factors between 1.0 and 2.0 in increments of 0.01 were then visually examined for expected collateralization patterns. SNR and the highest spatial weighting factor producing an accurate CBF territory map was calculated for ICAD patients with occlusions/aplastic vessels and three vascular territories ($n = 7$) as well as four healthy controls with either aplastic or hypoplastic A1 segments. Lastly, to account for potential variations in individual data, 0.1 was subtracted from each of these maximum spatial weighting factors.

Assessing circle of Willis variants in healthy volunteers

The purpose of this study in healthy controls was to assess the correspondence between CBF territory heterogeneity and anatomical variation in the circle of Willis. Only nonmixing CBF territory maps were examined in this analysis as DSA was not acquired in healthy controls. The diameters of circle of Willis vessels were measured on MRA and grouped into the following categories: right and left A1 segment of the anterior cerebral artery (ACA) present, absent, or hypoplastic (<1 mm)[15]; right and left posterior communicating artery (PCOM) present, absent, or fetal type; right and left P1 segment of the PCA present or absent. Fetal type was defined as a PCOM luminal diameter equal to or larger than the diameter of the ipsilateral P1 segment. *Cross-territorial indices* were calculated for each healthy control and assigned to their corresponding circle of Willis categories (i.e. RICA overlapping with LICA and LICA overlapping with RICA *cross-territorial indices* for A1 segment diameters). The results of this analysis were then plotted on a bar graph.

DSA comparison study in ICAD subjects

The purpose of this study in ICAD subjects was to compare CBF territory maps, which were expected to be asymmetric as they were acquired in ICAD patients with advanced stenoses and/or occlusions, with gold standard DSA. Validation of VE-pCASL territory maps in patients was assessed by initially comparing nonmixing CBF territory maps with perfusion on DSA according to the Alberta Stroke Program Early CT Score (ASPECTS) criteria. Specifically, each hemisphere was divided into 10 anatomic sites corresponding to the major intracranial arterial segments (A1,2; M1-6; P1,2), similar to Chng et al.[8] Perfusion was characterized on nonmixing CBF territory maps and DSA into the following categories, according to the one which prevailed for each anatomic site: 0 = no flow; 1 = collateral flow from other territory; 2 = normal antegrade flow. Nonmixing CBF territory maps were used initially as the visualization of predominant collateralization patterns in the presence of occlusions/absent vessels was the primary goal. Ten of 34 patients underwent DSA (see Table 1) and were included in this analysis (mean $\pm$ standard error: age $= 54.5 \pm 3.9$; sex = 7 M/3F). Angiographic data were graded by two raters: a board-certified neuroradiologist (MKS) and vascular neurosurgeon (MRF). Both raters were blinded to clinical history. Intrarater and interrater Cohen's *k*-statistics were calculated for APSECTS assignments on DSA and CBF territories between the two observers to test the hypothesis that independent readers could reliably interpret circle of Willis territory maps. Cohen's *k*-statistics ≥ 0.80 corresponded to very good agreement, whereas $0.60 < k < 0.80$ corresponded to good agreement.[16]

Mixing CBF territory maps were also examined using the same method of dividing hemispheres into 10 anatomical sites according to ASPECTS criteria. Perfusion was characterized on DSA into the following categories: 0 = no flow; 1 = partial contribution of flow to any portion of the territory from two or more vascular sources; 2 = collateral flow from other territory; 3 = normal antegrade flow. On CBF territory maps, mixing was readily identified based upon voxel colors. Lastly, the extent to which the external carotid artery (ECA) contributed to the major vascular CBF territories was also examined on DSA.

Flow territory correspondence with vasculopathy extent in ICAD subjects

The purpose of this study was to determine the robustness of CBF territory maps across all ICAD subjects in light of the fact that MRI data quality is expected to be more heterogenous in this population with advanced cerebrovascular disease. For subjects with occlusions without distal recanalization or collateralization via proximal branches, we hypothesized that we could readily identify corresponding asymmetric CBF territory maps either as a result of flow deficits or cross-territorial collateralization.

To quantitatively determine the degree of patient CBF territory map asymmetry relative to the standard CBF territory map, a single measure was calculated per subject based upon the extent of voxel overlap. Specifically, for each of the three CBF territories, the number of voxels belonging to a different CBF territory in the standard CBF territory map was divided by the total number of voxels in the standard CBF territory map to obtain a percentage. Only voxels present in both CBF territory maps were considered. This value was averaged across all three CBF territories to yield a single measure, which we term the *asymmetry index*. *Asymmetric indices* were subsequently grouped by moderate (50–69%) or severe (70–100%) stenosis (see Table 1).

A one-sided Mann–Whitney U test was performed to test whether the severe stenosis group had greater *asymmetric indices* relative to the moderate stenosis group. Additionally, a one-tailed z-score test for two proportions was performed to determine whether the ratio of voxels between ICA territories in controls (such that the ratio ≤ 1.0) was greater than the affected ICA/unaffected ICA ratio in ICAD subjects; subjects with primary VBA stenosis were not included in this analysis.

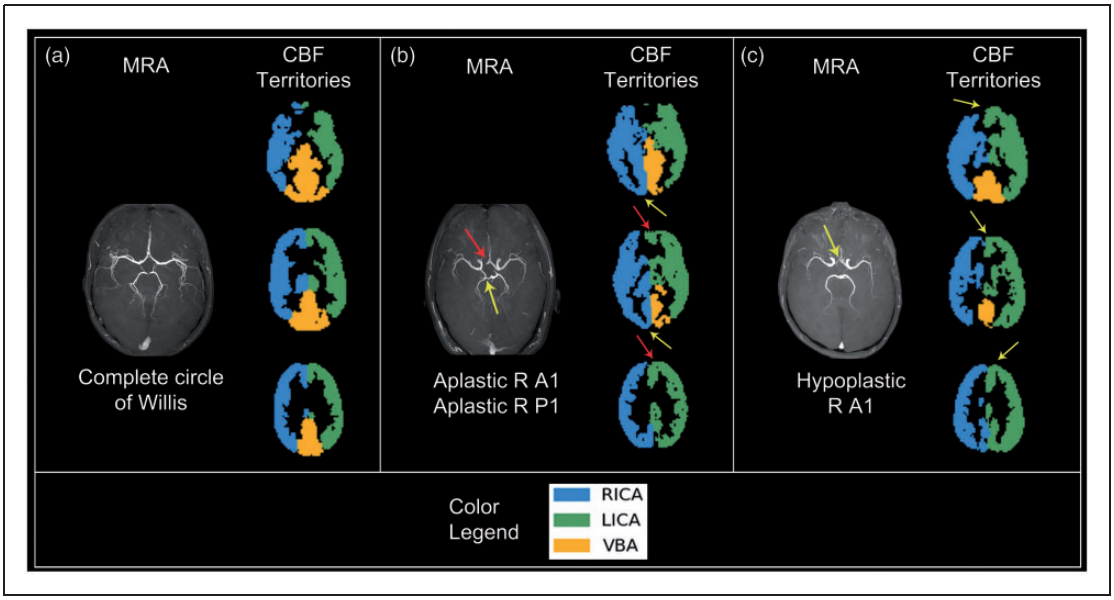

Figure 2. Qualitative comparison between MRA and CBF territory maps in healthy controls. (a) A complete circle of Willis is seen on MRA. The CBF territories closely resemble the standard CBF territory map. (b) An absent right A1 segment of the ACA (red arrow) and absent right P1 segment of the PCA (yellow arrow, only the superior cerebellar artery can be seen) is visualized on MRA. The CBF territory map shows that the right ACA territory is collateralized by the left ICA (red arrows) and that the right PCA territory is perfused from the right ICA (yellow arrows). (c) Hypoplastic right A1 segment of the ACA (yellow arrow) is seen on MRA. The corresponding CBF territories demonstrate left ICA perfusion supplying the right ACA territory (yellow arrows).

Results

Optimization of spatial weighting

SNR values (mean ± standard error) for healthy controls and ICAD patients were 7.49 ± 0.77 and 4.18 ± 0.28, respectively. When examining the seven ICAD patients with occlusions/absent vessels and three vascular territories as well as the three controls with aplastic or hypoplastic A1 segments, there was a marked increase in the maximum spatial weighting factor producing an accurate CBF territory map in patient CBF territory maps ($n = 5$; mean ± standard error: $SNR = 4.01 \pm 0.54$, spatial weighting factor $= 1.43 \pm 0.03$) relative to control maps ($n = 4$; mean ± standard error: $SNR = 7.96 \pm 0.48$, spatial weighting factor $= 1.23 \pm 0.03$). To account for the effect of SNR on spatial weighting, spatial weighting factors were subsequently assigned to 1.2 for $SNR < 6$ and 1.4 for $SNR > 6$. Of note, two ICAD patients were not included in this analysis due to spatial weighting factors not having an effect on the CBF territory maps. One of these patients had an infarct and loss of ASL signal corresponding to P2 occlusion without collateralization to this region, and the other patient with bilateral fetal-type PCOMs erroneously demonstrated CBF territories corresponding to a complete circle of Willis for all spatial weighting factors (*Patient seven*, see below).

Assessing circle of Willis variants in healthy volunteers

Seven of 10 healthy controls had a complete circle of Willis; two controls had fetal-type PCOMs and one had aplastic right A1 and P1 segments. CBF territory maps for three representative healthy volunteers with varying circle of Willis morphology, including MRA data, are shown in Figure 2.

Consistent with circle of Willis anatomy in our volunteer cohort, differences can be visualized graphically when ICA overlapping with contralateral ICA *cross-territorial indices* was grouped into present ($n = 16$), hypoplastic ($n = 3$), and absent ($n = 1$) A1 size categories as shown in Figure 3(a). Figure 3(b) shows that when ICA overlapping with VBA *cross-territorial indices* is averaged across present ($n = 19$) and absent ($n = 1$) P1 vessel size categories, a clear separation emerges as expected. A similar pattern of distinction can be seen in Figure 3(c) when PCOM sizes are separated into present ($n = 16$), fetal-type ($n = 3$), and absent ($n = 1$) size categories. Of note, statistical significance could not be established for this data as a result of the low number of subjects in some of the categories.

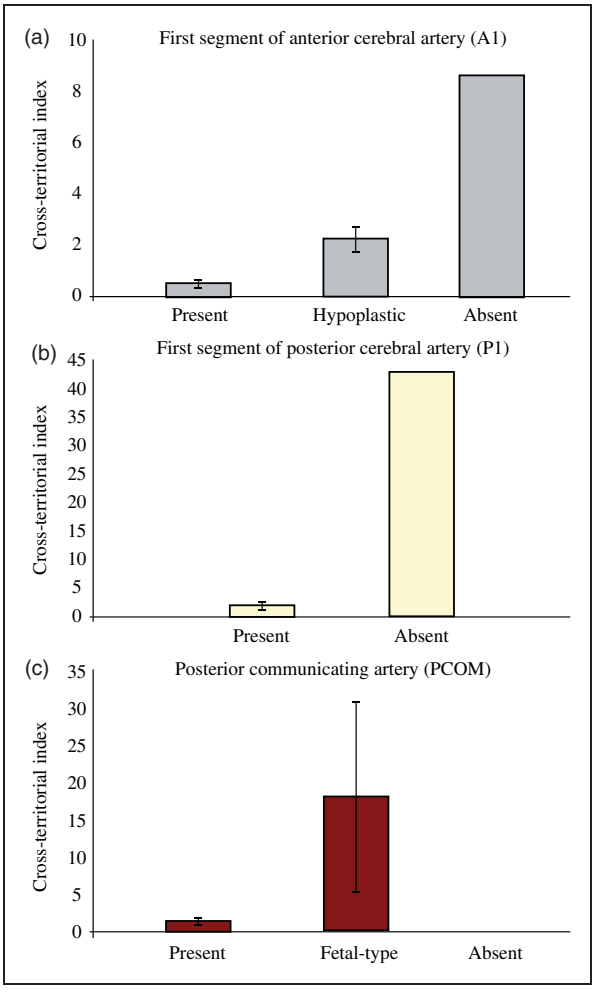

Figure 3. (a) When sizes of the A1 segment of the ACA are grouped into three categories (present, hypoplastic, and absent), there is an observable difference between the corresponding mean *cross-territorial indices* for ICA–ICA overlap across hemispheres. (b–c) Similarly, when sizes of the P1 segment of the PCA and PCOM are grouped, there is an observable difference between the corresponding mean *cross-territorial indices* for ipsilateral ICA–VBA overlap. Note: the scale of the y-axis is different between graphs.

DSA comparison study in ICAD subjects

CBF territory maps along with representative DSA images for ICAD subjects with intracranial artery occlusions/aplastic vessels are shown in Figure 4. Each of the subjects in this figure had unique collateralization patterns that are clearly identifiable on the CBF territory maps. Intrarater Cohen's *k*-statistics between perfusion assignments on DSA and CBF territories were 0.730 (95% CI = 0.593–0.867) and 0.708 (95% CI: 0.561–0.855) for reader one and reader two, respectively. Interobserver Cohen's *k*-statistics between CBF territory maps and DSA images were 0.819 (95% CI: 0.697–0.941) and 0.770 (95% CI: 0.633–0.907), respectively. All Cohen's *k*-statistics were greater than 0.60, and thus were considered to be in substantial agreement.[16] Mixing CBF territory maps were also generated using the fuzzy *c*-means algorithm in ICAD patients that underwent DSA (n = 10). Images comparing DSA with mixing CBF territory maps are shown for three select patients in Figure 5. Five patients underwent dedicated ECA injections and only one patient had detectable perfusion from ECA to the MCA territory, which was determined to be a small contribution from the left ECA to the left M5 APECTS region.

Flow territory correspondence with vasculopathy extent in ICAD subjects

CBF territory maps were of diagnostic quality in 33 of 34 subjects (97.1%); one patient (without DSA) was not included due to motion that was uncorrectable. As shown in Table 1, intracranial stenosis was 50–69% in 12 patients (mean *asymmetry index* $\pm$ SE = 3.8 $\pm$ 0.4) and 70% or greater in 21 patients (excluding the patient with head motion, mean *asymmetry index* $\pm$ SE = 8.4 $\pm$ 1.5). Individual patient *asymmetry indices* are also shown in Table 1. A one-sided Mann–Whitney U test revealed that ICAD patients with severe stenosis had significantly larger *asymmetry indices* relative to patients with moderate stenosis ($p = 0.026$). A one-tailed z-score test for two proportions to test whether the ratio of voxels between the left and right ICA territories in controls was greater than the affected ICA/unaffected ICA ratio in ICA stenosis patients trended toward statistical significance ($p = 0.085$).

There were seven patients with occlusions or aplastic circle of Willis vessels that did not undergo DSA. *Patient one* had an occluded right P2 segment (of the PCA) and right PCA infarct on FLAIR with an ASL signal deficit in the corresponding region on the CBF territory map (Figure 6(a)). *Patient two* had an occluded/aplastic right A1 segment with an intact anterior communicating artery (ACOM), large left A1 segment, and hypoplastic right PCOM and thus presumed collateralization of the entire right ACA territory by the LICA distribution, as demonstrated on the CBF territory map (Figure 6(b)). *Patient three* had an occluded/absent right P1 segment and an intact right PCOM; the right PCA territory was perfused by the RICA territory on the CBF territory map (Figure 6(c)). *Patient four* had a left fetal PCOM with perfusion provided to the left PCA territory by the ipsilateral ICA territory via the left PCOM (Figure 6(d)). *Patient five* had LICA occlusion with CTA revealing a large left PCOM without an identifiable ACOM; the CBF territory map showed perfusion of the entire left hemisphere by the VBA alone (Figure 6(e)).

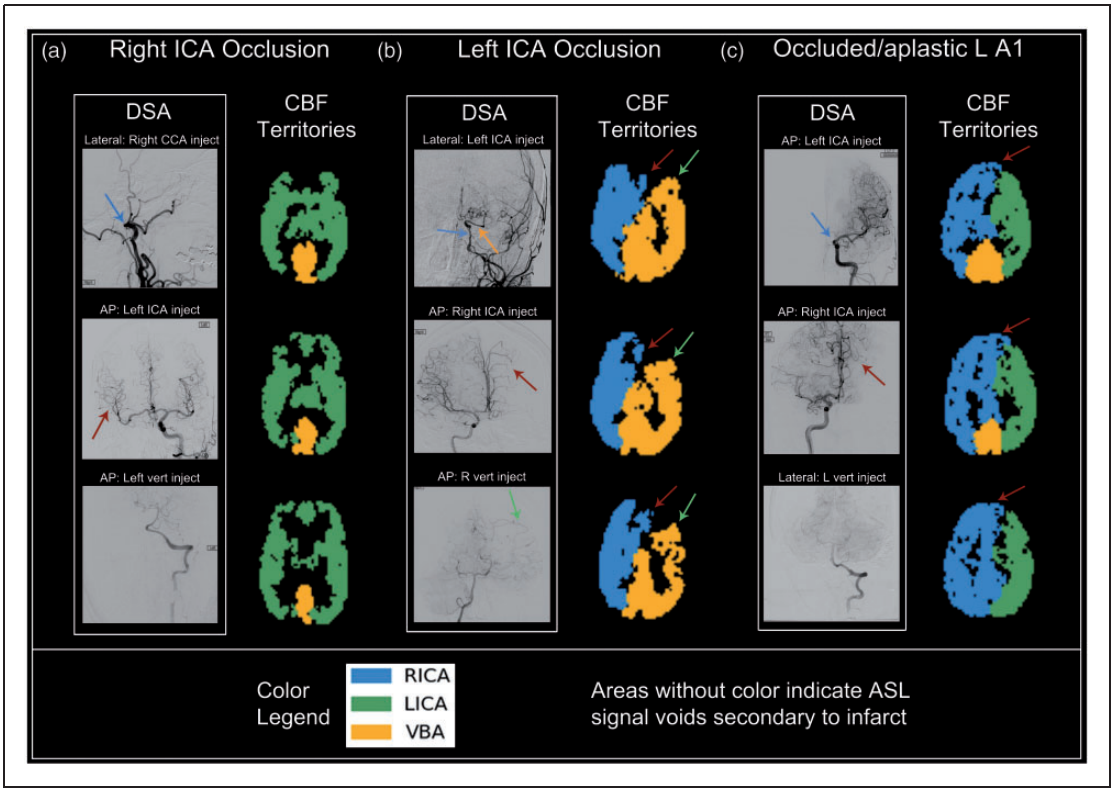

Figure 4. Qualitative comparison between DSA and CBF territory maps in patients with intracranial stenosis and occlusion. Subtitles above DSA images are formatted as *View (AP or lateral): Injection site*. (a) 68 y/o M: DSA demonstrates complete occlusion of the right ICA near the skull base (blue arrow, top DSA image) with collateral supply from the LICA distribution (red arrow, middle DSA image). The corresponding CBF territory map demonstrates filling of the entire anterior circulation by the left ICA. Posterior circulation is normal (bottom DSA image). (b) 62 y/o F: DSA showing severe multifocal stenosis of the left ICA (blue arrow, top DSA image) with near complete occlusion of the intracranial ICA both proximal and distal to the patent ophthalmic artery origin (orange arrow, top DSA image) with collaterals to the left ACA distribution from the RICA territory (red arrow, middle DSA image) and collaterals to the left MCA distribution from the VBA (green arrow, bottom DSA image). CBF territory maps reflect this perfusion pattern (red arrows and green arrows correspond to RICA and VBA collateralization, respectively). (c) 51 y/o M: DSA reveals occlusion/absence of the left proximal A1 segment (blue arrow, top DSA image) with collateral filling of the left A1 region from the RICA (red arrow, middle DSA image). The corresponding CBF territory map is in agreement with the DSA findings (red arrows correspond to RICA cross-filling of LICA territory). Flow from the VBA does not extend into the ICA territories (bottom DSA image).

There were also two subjects in whom CBF territory maps may not have corresponded to the most likely flow patterns as predicted by CTA (hereby referred to as questionable CBF territory maps). *Patient six* had an occluded/aplastic right A1 segment with an intact ACOM; however, the CBF territory map showed cross-filling from the LICA territory to only the posterior region of the right ACA territory as expected, whereas the anterior region of the right ACA territory remained supplied by the RICA territory (Figure 6(f)). *Patient seven* had bilateral fetal-type PCOMs with presumed perfusion of the PCA territories predominantly by the ICAs bilaterally; however, the CBF territory map revealed a perfusion pattern corresponding to a complete circle of Willis (Figure 6(g)). The remaining patients without occlusions or aplastic vessels did not demonstrate any significant asymmetry in their CBF territories aside from ASL signal dropout related to infarcts.

Discussion

Our results support the feasibility of a semiautomated, noninvasive MRI sequence for quantifying CBF and evaluating CBF territories in patients with clinically significant intracranial stenosis secondary to atherosclerotic disease. Perfusion patterns on CBF territory maps strongly correlated with angiographically confirmed intracranial anatomy and stenoses in controls and patients, respectively, with marked CBF territory asymmetry reflecting aplastic vessels or arterial occlusions.

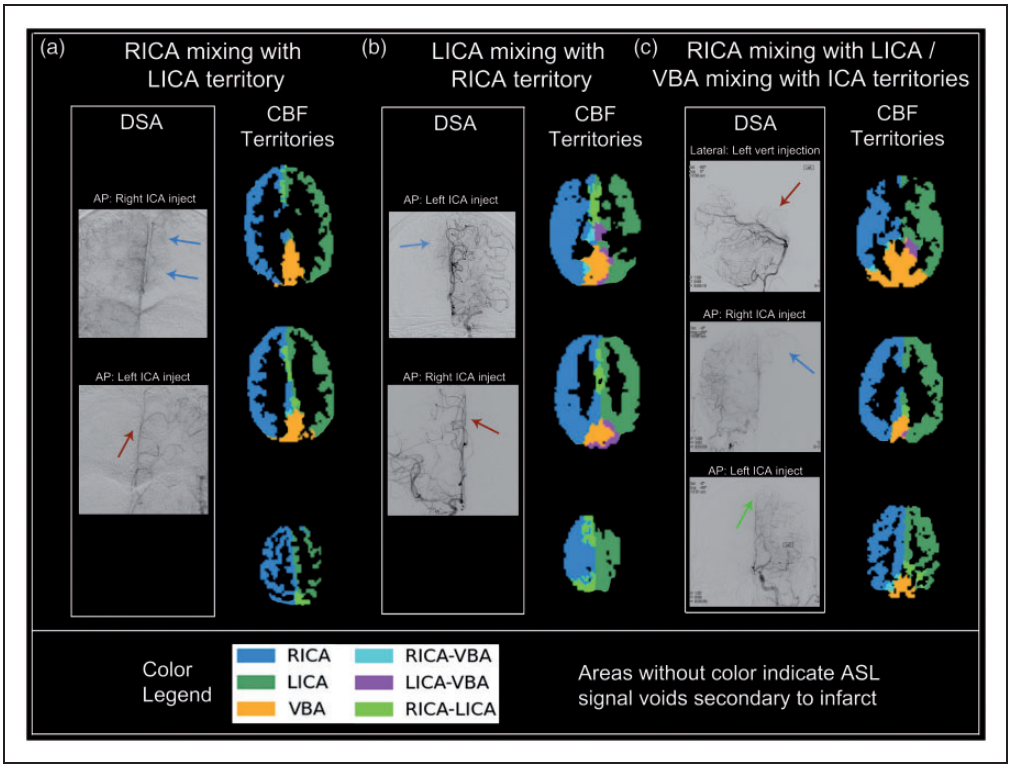

Figure 5. Qualitative comparison between DSA and mixing CBF territory maps in three representative ICAD patients. Subtitles above DSA images are formatted as *View (AP or lateral): Injection site*. (a) 51 y/o M: DSA reveals that the RICA cross-fills the left A1 segment territory (blue arrows, top DSA image), and that the LICA fills the left A1 segment normally (red arrow, bottom DSA image). This region of mixed perfusion in the left A1 territory can be seen on the mixing CBF territory maps (bright green clusters). (b) 64 y/o F: DSA shows that the LICA cross-fills the right A1 segment territory (blue arrow, top DSA image), and that the RICA fills the right A1 segment normally with no cross-filling on the left (red arrow, bottom DSA image). The region of mixed flow is seen on the mixing CBF territory maps (bright green clusters). Mixing between the ICAs and VBA is also seen. (c) 51 y/o M: DSA shows the basilar artery cross-filling the LICA territory (red arrow, top DSA image). The corresponding CBF territory map demonstrates mixing between the LICA and VBA territories (purple cluster). DSA (bottom two images) also shows cross-filling of the LICA territory by the RICA (blue arrow, middle DSA image), with the LICA territory also being perfused normally by the LICA (green arrow, bottom DSA image). The region of mixed flow is seen on the CBF territory maps (bright green clusters).

The application of ASL to patients with occlusions of major feeding arteries was first demonstrated by Hendrikse et al.[17] Around this time, selective pulsed ASL was introduced[18] and further refined,[19] although a clinically feasible method that did not rely upon extensive planning was not available until the VE-pCASL protocol proposed by Wong.[20] However, to date no study to our knowledge has validated planning-free VE-pCASL with DSA in a cohort of patients with cerebrovascular stenosis. To accurately determine CBF territories, our approach relied upon *k*-means clustering, similar to prior VE-pCASL studies,[18,19] as well as fuzzy *c*-means clustering to identify mixing between territories. These analyses use both the information encoded in the tagging efficiencies of each labeling scheme and the probability that a voxel belongs to each flow territory to formulate territory assignment decisions. While preparing and performing such calculations can be time consuming, we used freely available software to visualize CBF territories within minutes on the scanner console.

Alternative postprocessing schemes have been proposed, including pseudoinversion of an encoding matrix based upon tagging efficiencies[20] as well as Bayesian analyses.[21,22] A distinct advantage of the latter approach is the ability to determine the exact vascular sources underlying areas with mixed perfusion; such knowledge may assist in identifying the vessels supplying cerebrovascular pathology such as tumors and arteriovenous malformations. However, a potential drawback of the Bayesian method is the need to input prior information, including estimations of vessel location and flow, which may limit the robustness of CBF territory estimations particularly in patient populations with varying degrees of cerebrovascular disease; furthermore, using MRA or other angiographic data to determine vessel locations require extra time and planning, making it more difficult to implement on a

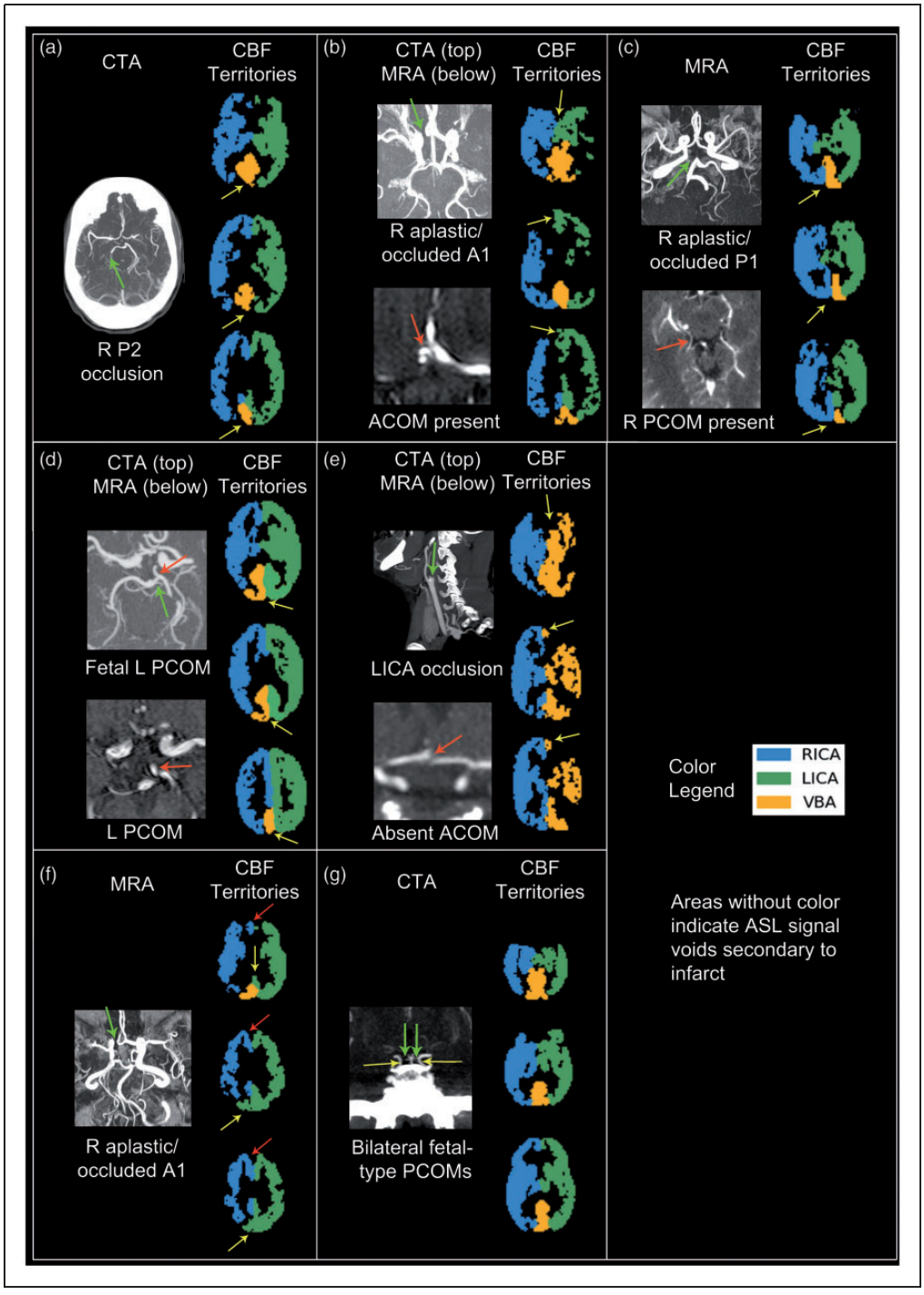

Figure 6. Qualitative comparison showing good correlation between CTA/MRA and CBF territory maps in patients with intracranial artery occlusion. (a) 75 y/o F: CTA demonstrates occlusion of the right P2 segment of the PCA (green arrow). CBF territory maps do not have ASL signal in this corresponding region (yellow arrows), signifying infarct. (b) 57 y/o M: CTA demonstrates a right aplastic/occluded A1 segment of the ACA (top image, green arrow). MRA also shows a large ACOM (bottom image, red arrow). CBF territories demonstrate perfusion of the right A1 segment by the left ICA territory region (yellow arrows), presumably through the ACOM. (c) 53 y/o F: MRA shows a right aplastic/occluded P1 segment of the PCA (top image, green arrow; of note, there is a vein underlying the same area). MRA also shows a patent right PCOM (bottom image, red arrow). CBF territory maps show a clear demarcation between the right and left hemisphere in the VBA territory, with flow supplied to the right VBA territory (yellow arrows) by the right ICA territory, presumably through the PCOM. (d) 72 y/o M: CTA shows a small left P1 segment of the PCA (green arrow) with a large left fetal-type PCOM (red arrow, top and bottom image). CBF territory maps shows perfusion of the left side of the VBA

broader clinical scale. Along with more novel postprocessing algorithms, newer VE-pCASL sequences have also recently been introduced. One such protocol minimizes the number of encoding cycles required via a rapid and automated optimized encoding scheme, improving the speed and robustness of VE-pCASL for a spectrum of possible vessel tagging scenarios.[23] Similarly, time-delay corrections have been used with nonparametric methods to account for delayed tagged blood arrival times.[24] Another promising protocol uses a multidelay VE-pCASL with background suppressed 3D GRASE to better account for variable arterial transit times in patients with severe intracranial stenosis.[25] Future testing is required to determine the reliability with which these proposed methods can be applied to cohorts of patients with severe stenoses and occlusions.

We were able to achieve robust, angiographically confirmed CBF territory results in the majority of participants. To account for the smaller SNR of ICAD patient MRI datasets relative to healthy control datasets, spatial weighting factors were assigned to 1.2 for $SNR < 6$ and 1.4 for $SNR > 6$. In doing so, we were able to improve the reliability of the results without over-weighting the data. One patient in our study did have substantial head motion, leading to nonphysiologic CBF territory assignments across the brain. Given these easily detected aberrant changes, this patient's data was not included in the final analysis. While head motion can be particularly problematic as labeling efficiencies can change throughout the duration of the scan leading to territorial misclassifications by the clustering algorithm, the scan duration was short (less than 5 min), preventing this from becoming a more common issue. Of note, we found that mixing involving the posterior circulation in particular was difficult to grade on DSA as there was increased subjectivity in determining whether more than one vascular source contributed significant perfusion to a given region, making group-wise analysis difficult. Furthermore, mixing on CBF territory maps often involved small, scattered clusters, which were difficult to validate on DSA. Nonetheless, good correlation was observed between DSA and mixing CBF territory maps in cases involving the anterior circulation in particular.

There may be several reasons why the two patients described in "Results" section had CBF territory maps that did not entirely correspond with flow territories that were expected by MRA/CTA. *Patient six* with a right aplastic/occluded A1 segment and intact ACOM had cross-filling to the posterior, but not the anterior, portion of the right ACA territory on the CBF territory map. As DSA was not available, it was not possible to determine whether alternative routes such as ipsilateral leptomeningeal anastomoses between middle and anterior cerebral arteries[2] existed in this patient, and the degree to which such routes provided collateral perfusion. *Patient seven* with bilateral fetal-type PCOMs did not demonstrate the expected amount of PCA territory collateralization from the anterior circulation to regions superior to the cerebellum, although the very small P1 segments may have still supplied a small amount of flow to this region. We initially postulated that this CBF territory misrepresentation was due to over-weighting the VBA territory relative to the anterior territories; however, decreasing the spatial weighting factor did not affect CBF territory patterns to any significant degree. Future work will seek to determine how to more accurately represent collateralization in the setting of bilateral fetal-type or fetal PCOMs. Nonetheless, in the case of unilateral absent/occluded P1 segments, CBF territory maps consistently reflected collateralization from the ipsilateral ICA territory.

The utility of a VE-pCASL approach for mapping CBF territories includes the detection of primary collateral flow through the circle of Willis as well as more distal secondary pathways. Results derived from VE-pCASL protocols are more sensitive relative to traditional modalities like MRA in identifying distal pathways that may serve as important conduits for preserving CBF.[26] Currently, the only other modality that can reliably detect smaller and more distal collateral pathways is DSA. Another benefit of mapping CBF territories is that visualization of the source of perfusion is very straightforward, particularly when these maps are overlaid on an anatomical atlas. By combining this ASL-derived information with vascular patterns identified on DSA, it is possible to better characterize unique perfusion patterns. In future studies, we

Figure 6. Continued
territory by the left ICA territory (yellow arrows), presumably through the left PCOM. (e) Sagittal CTA image shows abrupt cutoff of the left ICA (top image, green arrow). Axial MRA image does not reveal an ACOM (bottom image, red arrow). CBF territory maps show perfusion of the entire left hemisphere by the VBA territory alone (yellow arrows); the right ICA territory does not supply the left A1 region if no ACOM exists. (f) MRA demonstrates an aplastic/occluded A1 segment of the right ACA (green arrow). CBF territory maps reveal that only the posterior right A1 region receives supply from the left ICA territory (yellow arrows), although collaterals from the left ICA territory to the anterior right A1 region (red arrows) would also be expected. (g) CTA shows bilateral fetal-type PCOMs (yellow arrows) and small P1 segments (green arrows). The CBF territory map shows a complete Circle of Willis configuration, although minimal perfusion from the posterior circulation above the cerebellum would be expected.

will seek to determine whether shifting of CBF territories during the administration of a vasoactive agent relative to room air is more prominent in patients that experience future strokes, further lending its utility as a potentially important risk biomarker.

It should be noted that with the implemented clustering analysis approach, the vessel-encoded images are only used to determine the vascular source(s) of each voxel. Therefore, unlike control and global label images, vessel-encoded images have no effect on CBF quantification. The location of additional arteries, such as the ECA within the labeling plane, is irrelevant with regards to CBF estimation as all blood passing through the labeling plane should be labeled with the same efficiency. Exceptions to this possibility include when the velocity of such an artery is markedly different from the carotids or when the artery is highly tortuous at the labeling plane; in such cases, the labeling efficiency may be very low. With the vessel-encoded approach all vessels are labeled or controlled simultaneously, so any other vessels present in the labeling plane will be encoded in some fashion regardless of their proximity to the primary arteries of interest and will be assigned to one of the major feeding arteries. For example, due to the periodicity of the encodings, an artery to the right of the right ICA (e.g. the right ECA) could be encoded in exactly the same manner as the left ICA, making these two arteries indistinguishable after post-processing despite their physical distance in the labeling plane. In subjects where DSA data were available, we confirmed that there was no substantial contribution from the ECA to the ICA flow territories. However, the ECA contribution in subjects outside of our study may still be significant. In such patients, it will likely be necessary to employ alternative labeling strategies to measure the ECA contribution more specifically.[27]

The current study has several potential limitations which may motivate future studies. First, only a single postlabeling delay was employed before data acquisition, which may be problematic in a population of ICAD patients. Specifically, flow in cortical watershed regions where perfusion gradually shifts should be interpreted with caution, particularly in regions with asymmetric CBF territories. In addition, flow through small vessels such as leptomeningeal collaterals will also be delayed which may affect CBF territory results. Consequently, we utilized a long labeling duration of 1650 ms followed by a labeling delay of 1600 ms, allowing substantial time for blood to arrive to the tissue before acquisition. However, longer preacquisition delays also lead to more pronounced magnetization decay and affect CBF territory results, and thus future analyses could implement the methods mentioned previously to address this issue. For the current study, the number of CBF territories had to be chosen manually; future work will seek to determine this number automatically using a measure such as the gap statistic.[28] With regards to the nature of the spatially selective labeling, substantial labeling may have persisted for 5–10 mm beyond the vessel being labeled. However, given the general distance between the ICAs and VBA vessels at this location (25–50 mm for ICAs; 10–15 mm for ICAs and VBAs), we expect that this spillover effect is small. A final potential limitation of our study was that radiofrequency labeling occurred 90 mm below the corpus collosum. Prior studies have revealed that the ECA branches from the common carotid artery as high as the hyoid bone[29]; thus, labeling was performed distal to the carotid bifurcation in all participants except in those with unusual anatomy. However, tagging of the ECA still may have occurred if it coursed adjacent and approximately parallel to the ICA at the tagging plane. Except for the aforementioned circumstance, perfusion may have been underestimated in patients with severe ICAD in particular as the ECA can serve as an important collateral pathway in severe ICAD.[30] Consequently, future studies may perform RF tagging at a site proximal to the carotid bifurcation in order to both examine the contribution of the ECA to cerebral perfusion as well as to examine CBF collateralization patterns in the setting of more proximal ICA and vertebral artery disease.

In summary, we used angiographic studies to validate a planning-free, noninvasive semiautomated pipeline for deriving CBF quantitatively and visualizing CBF territories in both healthy controls as well as a large patient cohort with varying levels of atherosclerotic intracranial disease, including large-vessel occlusions. These results support the feasibility of a semiautomated pipeline for evaluating major neurovascular CBF territories in patients with ICAD.

Funding

The author(s) disclosed receipt of the following financial support for the research, authorship, and/or publication of this article: American Heart Association (14GRNT20150004) and National Institutes of Health (1R01 NS097763).

Declaration of conflicting interests

The author(s) declared no potential conflicts of interest with respect to the research, authorship, and/or publication of this article.

Authors' contributions

DFA performed analysis and interpretation of the data, and wrote the paper. MKS, MRF, CCF, LTD, and BAR performed analysis and interpretation of the data, and assisted in revision of the manuscript. AOS assisted with acquisition of the data. MJD designed the experiment and acquired the data, assisted with analysis and interpretation of the data, and wrote the manuscript.

Supplementary material

Supplementary material for this paper can be found at http://jcbfm.sagepub.com/content/by/supplemental-data

References

1. Holmstedt CA, Turan TN and Chimowitz MI. Atherosclerotic intracranial arterial stenosis: risk factors, diagnosis, and treatment. *The Lancet Neurol* 2013; 12: 1106–1114.
2. Liebeskind DS. Collateral circulation. *Stroke* 2003; 34: 2279–2284.
3. Liebeskind DS, Cotsonis GA, Saver JL, et al. Collateral circulation in symptomatic intracranial atherosclerosis. *J Cerebr Blood Flow Metab* 2011; 31: 1293–1301.
4. Alsop DC, Detre JA, Golay X, et al. Recommended implementation of arterial spin-labeled perfusion MRI for clinical applications: a consensus of the ISMRM perfusion study group and the European consortium for ASL in dementia. *Magn Reson Med* 2015; 73(1): 102–116.
5. Hartkamp NS, Helle M, Chappell MA, et al. Validation of planning-free vessel-encoded pseudo-continuous arterial spin labeling MR imaging as territorial-ASL strategy by comparison to super-selective p-CASL MRI. *Magn Reson Med* 2014; 71: 2059–2070.
6. Donahue MJ, Hussey E, Rane S, et al. Vessel-encoded arterial spin labeling (VE-ASL) reveals elevated flow territory asymmetry in older adults with substandard verbal memory performance. *J Magn Reson Imaging* 2014; 39: 377–386.
7. Gevers S, Bokkers RP, Hendrikse J, et al. Robustness and reproducibility of flow territories defined by planning-free vessel-encoded pseudocontinuous arterial spin-labeling. *AJNR* 2012; 33: E21–E25.
8. Chng SM, Petersen ET, Zimine I, et al. Territorial arterial spin labeling in the assessment of collateral circulation: comparison with digital subtraction angiography. *Stroke* 2008; 39: 3248–3254.
9. Wu B, Wang X, Guo J, et al. Collateral circulation imaging: MR perfusion territory arterial spin-labeling at 3T. *AJNR* 2008; 29: 1855–1860.
10. Rosset A, Spadola L and Ratib O. OsiriX: an open-source software for navigating in multidimensional DICOM images. *J Digital Imaging* 2004; 17: 205–216.
11. Samuels OB, Joseph GJ, Lynn MJ, et al. A standardized method for measuring intracranial arterial stenosis. *AJNR* 2000; 21: 643–646.
12. Abraham A, Pedregosa F, Eickenberg M, et al. Machine learning for neuroimaging with scikit-learn. *Front Neuroinformat* 2014; 8: 14.
13. Dunn JC. A fuzzy relative of the ISODATA process and its use in detecting compact well-separated clusters. *J Cybernet* 1973; 3: 32–57.
14. Arthur D and Vassilvitskii S. K-means++: the advantages of careful seeding. In: *Proceedings of the eighteenth annual ACM-SIAM symposium on discrete algorithms*. Philadelphia, PA: Society for Industrial and Applied Mathematics, 2007, pp.1027–1103.
15. Liebeskind DS and Caplan LR. Anatomy of Intracranial Arteries. In: Kim JS, Caplan LR and Wong KSL (eds) *Intracranial Atherosclerosis*. Oxford: Wiley-Blackwell, 2008.
16. Sim J and Wright CC. The kappa statistic in reliability studies: use, interpretation, and sample size requirements. *Physical Therapy* 2005; 85: 257–268.
17. Hendrikse J, van Osch MJ, Rutgers DR, et al. Internal carotid artery occlusion assessed at pulsed arterial spin-labeling perfusion MR imaging at multiple delay times. *Radiology* 2004; 233: 899–904.
18. Davies NP and Jezzard P. Selective arterial spin labeling (SASL): perfusion territory mapping of selected feeding arteries tagged using two-dimensional radiofrequency pulses. *Magn Reson Med* 2003; 49: 1133–1142.
19. Hendrikse J, van der Grond J, Lu H, et al. Flow territory mapping of the cerebral arteries with regional perfusion MRI. *Stroke* 2004; 35: 882–887.
20. Wong EC. Vessel-encoded arterial spin-labeling using pseudocontinuous tagging. *Magn Reson Med* 2007; 58: 1086–1091.
21. Chappell MA, Okell TW, Jezzard P, et al. A general framework for the analysis of vessel encoded arterial spin labeling for vascular territory mapping. *Magn Reson Med* 2010; 64: 1529–1539.
22. Chappell MA, Okell TW, Payne SJ, et al. A fast analysis method for non-invasive imaging of blood flow in individual cerebral arteries using vessel-encoded arterial spin labelling angiography. *Med Image Anal* 2012; 16: 831–839.
23. Berry ES, Jezzard P and Okell TW. An optimized encoding scheme for planning vessel-encoded pseudocontinuous arterial spin labeling. *Magn Reson Med* 2015; 74(5): 1248–1256.
24. Donahue MJ, Strother MK, Lindsey KP, et al. Time delay processing of hypercapnic fMRI allows quantitative parameterization of cerebrovascular reactivity and blood flow delays. *J Cereb Blood Flow Metab*. Epub ahead of print 19 October 2015. DOI: 10.1177/0271678X15608643.
25. Wang DJ, Alger JR, Qiao JX, et al. Multi-delay multi-parametric arterial spin-labeled perfusion MRI in acute ischemic stroke – comparison with dynamic susceptibility contrast enhanced perfusion imaging. *NeuroImage Clin* 2013; 3: 1–7.
26. Qiao XJ, Salamon N, Wang DJ, et al. Perfusion deficits detected by arterial spin-labeling in patients with TIA with negative diffusion and vascular imaging. *AJNR* 2013; 34: 2125–2130.
27. Yu SL, Wang R, Wang S, et al. Accuracy of vessel-encoded pseudocontinuous arterial spin-labeling in identification of feeding arteries in patients with intracranial arteriovenous malformations. *AJNR* 2014; 35: 65–71.
28. Tibshirani R. Estimating the number of clusters in a data set via the gap statistic. *J R Stat Soc* 2001; 63: 411–423.
29. Al-Rafiah A, El-Haggagy AA, Aal IH, et al. Anatomical study of the carotid bifurcation and origin variations of the ascending pharyngeal and superior thyroid arteries. *Folia Morphol* 2011; 70: 47–55.
30. van Laar PJ, van der Grond J, Bremmer JP, et al. Assessment of the contribution of the external carotid artery to brain perfusion in patients with internal carotid artery occlusion. *Stroke* 2008; 39: 3003–3008.